Journal of Alloys and Compounds 474 (2009) 140–146

Contents lists available at ScienceDirect

Journal of Alloys and Compounds

journal homepage: www.elsevier.com/locate/jallcom

Hydrogen terminal solid solubility determinations in Zr–2.5Nb pressure tube microstructure in an extended concentration range

J.P. Giroldi, P. Vizcaíno*,[1], A.V. Flores, A.D. Banchik

LMFAE, Centro Atómico Ezeiza, Presbítero Juan Gonzáles y Aragón N° 15, B1802AYA Ezeiza, Buenos Aires, Argentina

ARTICLE INFO

Article history:
Received 11 May 2008
Received in revised form 20 June 2008
Accepted 24 June 2008
Available online 9 August 2008

Keywords:
Nuclear reactor materials
Thermodynamic properties
Thermal analysis
TEM

ABSTRACT

In the present work the temperature of terminal solid solubility of hydrogen in the zirconium alloy Zr–2.5Nb was measured for material taken from a CANDU type pressure tube. The measurements were made in a wide concentration range (50–463 wppm) using two techniques, differential scanning calorimetry and differential dilatometry, with the additional purpose of checking the coincidence of the TSS points in both techniques. The work was complemented by microstructural studies pursuing the (β-Zr) → (α-Zr + β-Zr_{enr} + β-Nb) transformation. This transformation is accelerated if the material remains at temperatures higher than 400 °C, which corresponds to a hydrogen solubility of about 180 wppm. Thus, microstructural studies were made by transmission electron microscopy and energy dispersive analysis, which allowed to relate changes in the solubility with these microstructural transformations.

1. Introduction

In the CANDU type reactors the fuel elements and the heavy water coolant are placed inside pressure tubes of the Zr–2.5Nb zirconium-based alloy. The severe operating conditions of this particular component: neutron radiation, internal pressures of about 115 atm, temperatures of 300 °C and an aqueous environment, make the study and monitoring of this component a topic of continuous concern. The main degradation factors, which affect the life of these components, are neutron radiation and hydrogen (deuterium) incorporation. As a consequence, delay hydrogen cracking (DHC) and microstructural evolution from the original structure occur.

In the present context, an accurate knowledge of the hydrogen solubility is a matter of continuous interest in Zr–2.5Nb. Nowadays, attention is given to a concentration range higher than the interval of 10–100 wppm, since the expectations are that pressure tubes will remain in service containing more than 100 wppm.

As it is known, the pressure tube lamellar microstructure of α-Zr plus β-Zr is methastable and evolves to α-Zr plus β-Nb precipitates under appropriate conditions. Then, in order to measure concentrations higher than 180 wppm, that is, for temperatures of terminal solid solubility (TTSS) higher than 400 °C, it is essential to consider the microstructural transformation (β-Zr) → (β-Zr_{enr} + ω) → (α + β-Zr_{enr} + ω) → (α + β-Zr_{enr}) → (α-Zr + β-Zr_{enr} + β-Nb) [1,2], which becomes faster if the material remains at these temperatures.

On the other hand, some disagreement exists in the literature in relation to the determination of this temperature by differential scanning calorimetry (DSC) and other techniques. Khatamian and Root, using DSC and neutron diffraction, ND, concluded that the most reliable point to measure the temperature of TTSS is the peak temperature (pT) in the calorimetric curve [3]. On the other hand Pan and Puls, using internal friction, IF, (Young modulus vs. temperature) and performing quasistatic thermal cycles arrived to the conclusion that the most reliable one is the maximum slope temperature (msT) [4].

In the present context there are enough motivations to increase the interval under consideration above the 100 wppm, to explore the level of transformation of the original microstructure during TSS determinations. This exploration should be carried out basically for samples containing more than 180–200 wppm using a second reference technique in order to contrast the usual criteria to determine TSS by DSC and IF.

This task was performed in the present work using DSC and differential dilatometry, DD, as a contrasting technique. Microstructural studies were carried out by transmission electron microscopy, TEM, and X-ray energy dispersive analysis, EDX, to determine the degree of β-Zr phase decomposition.

2. Materials

The material was obtained from a piece of pressure tube similar to the ones installed in the Embalse Nuclear Power reactor (CNE), Argentina. The lamellar

* Corresponding author. Tel.: +54 11 6779 8295; fax: +54 11 6779 8427.
E-mail address: vizcaino@cae.cnea.gov.ar (P. Vizcaíno).
[1] Also at the Carrera del Investigador from CONICET.

0925-8388/$ – see front matter © 2008 Elsevier B.V. All rights reserved.
doi:10.1016/j.jallcom.2008.06.104

Table 1
Thermal treatments performed for the TEM specimens

Sample batch	Thermal treatment (TT)
0	No TT
1	30 min at 400 °C
2	1 h 30 min at 550 °C
3	24 h at 550 °C

microstructure (α-Zr + β-Zr) of the material is the result of the pressure tube fabrication process, an extrusion at high temperatures (815 ± 10) °C followed by a cold work deformation (27%). The tube receives a stress relieve thermal treatment of 24 h at 400 °C under water steam in autoclave. The resulting microstructure is methastable, formed by two phases: α-Zr, the zirconium low temperature phase and β-Zr, unstable but in fact methastable at room temperature, enriched by niobium (20 wt.%).

2.1. Microstructure

The pressure tube microstructure is a lamellar structure composed by elongated α-Zr (hexagonal) grains in the axial direction (0.3–0.7 μm thick), containing 0.8 wt.% Nb and tiny β-Zr (cubic) bands surrounding the α-Zr grains (<0.1 μm thick, 10 times slighter than the α-Zr), which contains about 20 wt.% of Nb.

Due to in service conditions the β-Zr phase evolves in a decomposition process which leaves to a stable microstructure composed by the α-Zr and β-Nb (cubic) phases.

In order to check the microstructural evolution during the thermal cycles in the DD and DSC runs, some samples were prepared for TEM studies. These samples were thermally treated in the conditions shown in Table 1, equivalent to the DD and DSC thermal cycles.

2.2. Sample preparation for DD and DSC

Specimens of 20 mm × 5 mm × 2 mm were cut in the axial direction of the tube. The surfaces were polished with SiC paper and cleaned with acetone.

2.2.1. Hydrogen incorporation

Hydrogen incorporation was made in two stages:

(1) Initially, a hydride surface layer was deposited by the cathodic charge technique.
(2) An annealing to diffuse the hydrogen into the bulk.

2.2.1.1. Cathodic charge. The charging process was carried out in an electrolytic cell at 90 ± 1 °C circulating a current density of 15–25 mA/cm^2. The electrolyte was a 0.1 molar solution of H_2SO_4 in H_2O. The time of the process varied from 12 to 120 h, in order to obtain surface layers of different thickness.

2.2.1.2. Diffusive thermal treatment. It was made under a N_2 atmosphere during 24 h at 400 °C. In order to obtain samples with hydrogen concentrations higher than 180–200 wppm, a different number of thermal cycles were performed up to this temperature. Finally the samples were carefully polished with the aim to remove the oxide and any remaining hydride layer.

3. TSS temperatures determination

3.1. Dilatometry

The DD runs were performed in a differential dilatometer Shimadzu, model TMA 60-H, at a heating–cooling rate of ±5 °C/min from room temperature to 400 °C, or up to 550 °C for the samples having more than 180 wppm. The samples remained at this temperature for 30 min. The runs were made under a dynamic N_2 flux of 25 ml/min. Since it is a differential apparatus, a reference sample is needed. For this purposes, samples of similar dimensions were cut from the tube but without submitting them to the cathodic charge process. These samples contained about 10 wppm, which had been incorporated during the pressure tube fabrication process.

There are different criteria to measure the temperature of TTSS. In the dilatometric curves, the temperature of TTSS in dissolution, TTSSd, is normally determined in the point where the slope of the expansion curve changes abruptly during the heating stage. But in this particular alloy, Zr–2.5Nb, this point was not clearly defined for low hydrogen contents as in other zirconium alloys [5], then, it

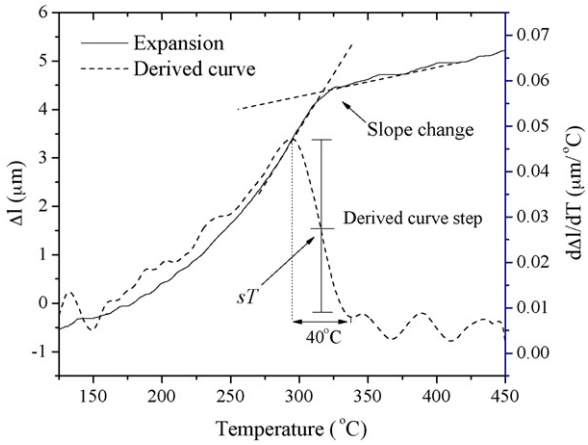

Fig. 1. Expansion curve during heating (hydride dissolution).

was necessary to differentiate the DD curve and measure TTSSd in the discontinuity (step) observed in the derived curve (step temperature, sT), Fig. 1. TTSSp was determined in the same manner, Fig. 2.

3.2. Calorimetry

The calorimetric experiments were made using a thermal flux DSC Shimadzu, model DSC-60. The dimensions of the samples were 4 mm × 4 mm × 2 mm. Two runs were performed to each sample at 5 °C/min, in order to compare with the dilatometric data obtained at the same rate, but the first one was discarded and TTSS were determined in the second run. All the experiments were carried out from room temperature to 400 or 550 °C. The runs were made under a pure N_2 dynamic atmosphere of 25 ml/min.

The TSS dissolution temperatures, TTSSd, were determined following the three criteria commonly observed in the literature [6]. Then, the peak, maximum slope and completion temperatures were measured. In the precipitation case, which begins after hydrogen saturation has occurred; a sharp peak at the onset of the process is observed. In this case, there is not a great difference between these three temperatures and this is the reason why we choose the pT as the unique criterion for TTSSp determinations, Figs. 3 and 4.

3.3. Hydrogen content determinations

After the DSC and DD runs, the samples were polished and washed with acetone again for the hydrogen determinations. These

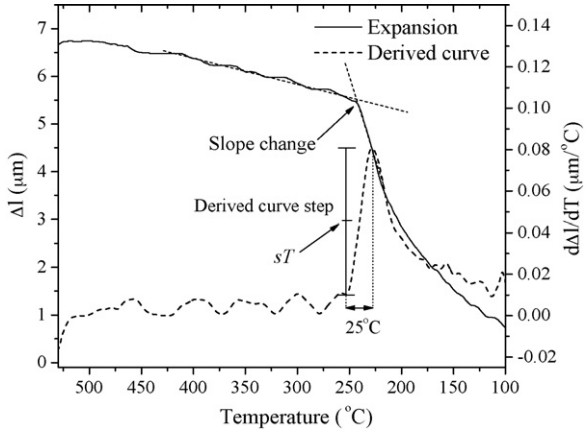

Fig. 2. Expansion curve during cooling (hydride precipitation).

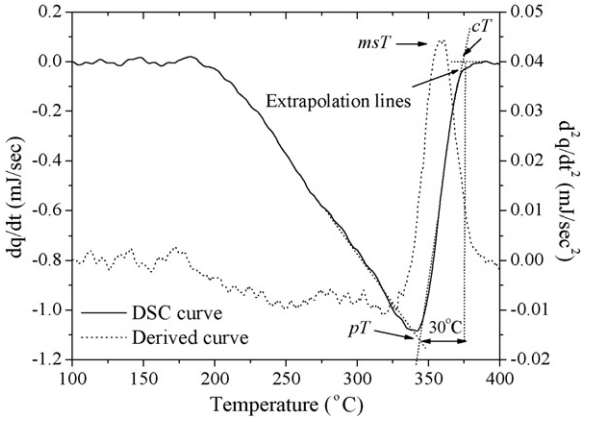

Fig. 3. Calorimetric curve in the heating stage. The points associated with TTSSd are indicated: peak temperature (pT), maximum slope temperature (msT) and completion temperature (cT).

measurements were made using a hydrogen gas meter LECO RH-404. The process consist of the sample melting and the extraction of the gasses which are transported by a carrier gas, separated by a chromatographic column and finally analyzed in a calibrated cell. The experimental error of these determinations is ±4 wppm.

4. Results

4.1. Dilatometry

As it was previously mentioned, TTSSd was measured in the middle step point of the derived expansion curve; sT. Using these data, the vant Hoff plot observed in Fig. 5 was made.

From the linear fitting the solubility curve and dissolution enthalpy were obtained:

$$C_H(\text{ppm}) = 6.89 \times 10^4 \exp\left(\frac{-3930}{T(\text{K})}\right); \quad (1)$$

$$\Delta H = 33 \pm 1 \text{ kJ/mol H}$$

The precipitation data are plotted in Fig. 6.The precipitation curve and the precipitation enthalpy are:

$$C_H(\text{ppm}) = 1.99 \times 10^4 \exp\left(\frac{-2768}{T(\text{K})}\right); \quad (2)$$

$$\Delta H = 23 \pm 1 \text{ kJ/mol H}$$

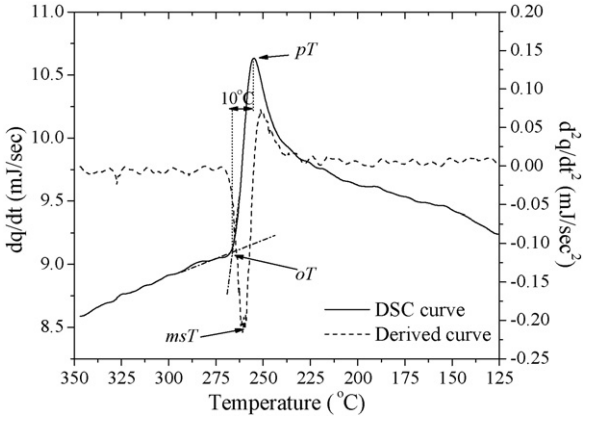

Fig. 4. Calorimetric curve in the cooling stage, the onset temperature (oT), maximum slope temperature (msT) and peak temperature (pT) are indicated.

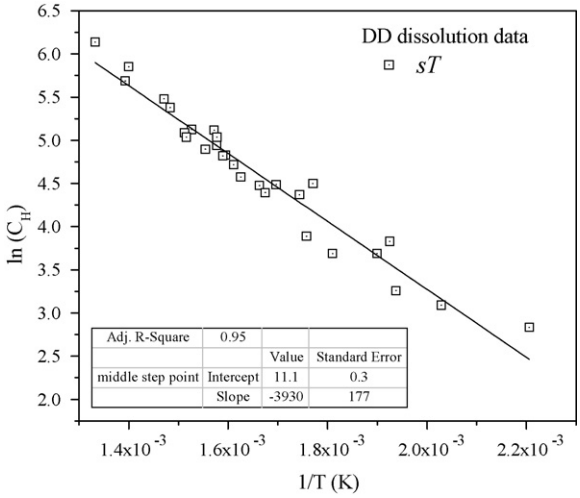

Fig. 5. vant Hoff plot made with the dilatometric dissolution data. The fit is good but a slight derive from linearity is observed for the highest temperatures.

4.2. Calorimetry

Fig. 7 shows the vant Hoff plots and linear regressions for the DSC data in dissolution. The data were obtained measuring pT, msT and cT.

The curves and the enthalpy values are:

$$\text{pT}: C_H(\text{ppm}) = 6.11 \times 10^4 \exp\left(\frac{-3827}{T(\text{K})}\right); \quad (3)$$

$$\Delta H = 32 \pm 1 \text{ kJ/mol H}$$

$$\text{msT}: C_H(\text{ppm}) = 5.26 \times 10^4 \exp\left(\frac{-3826}{T(\text{K})}\right); \quad (4)$$

$$\Delta H = 32 \pm 1 \text{ kJ/mol H}$$

$$\text{cT}: C_H(\text{ppm}) = 5.21 \times 10^4 \exp\left(\frac{-3883}{T(\text{K})}\right); \quad (5)$$

$$\Delta H = 32 \pm 1 \text{ kJ/mol H}$$

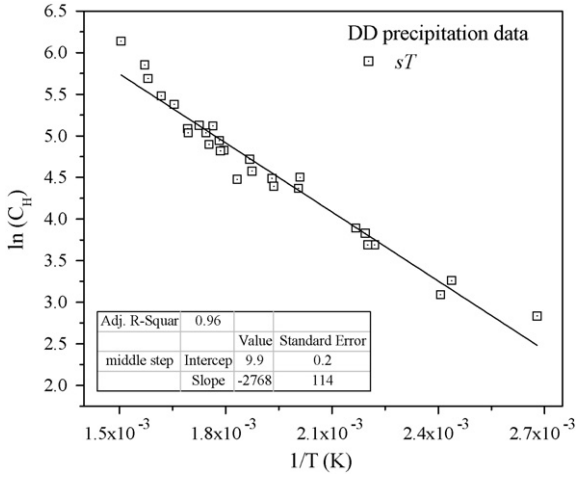

Fig. 6. vant Hoff plot made with the dilatometric precipitation data. The fit derives from linearity for the highest temperatures.

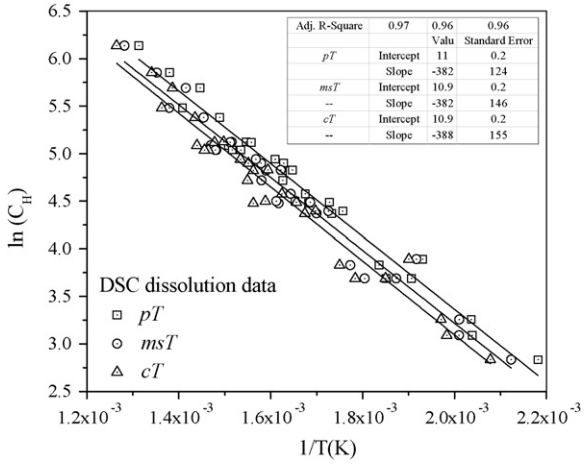

Fig. 7. vant Hoff plot made with the DSC dissolution data. The linear regressions were obtained measuring pT, msT and cT.

Fig. 8 shows the vant Hoff for the DSC precipitation data.

The precipitation curve and enthalpy are:

$$C_H(\text{ppm}) = 2.22 \times 10^4 \exp\left(\frac{-2961}{T(\text{K})}\right); \quad (6)$$

$$\Delta H = 25 \pm 1\ \text{kJ/mol H}$$

5. Discussion

5.1. Dissolution

DD proved to be less accurate than the DSC for the TTSS determinations. The uncertainty in TTSS dilatometric measurements was evaluated between 5 and 6 °C.

In the calorimetric experiments, TTSS is measured in the baseline recovery region of the curve. Even though DSC data were more accurate than DD data (the uncertainty is smaller than 2 °C), the criterion selected to determine TTSS affects the results considerably. In fact, the temperature interval from pT to cT in dissolution fluctuates between 25 and 30 °C in the conditions of the present work, as can be see in a qualitative form in Fig. 3.

In the last few years, two works developed this matter arriving to different conclusions. The first one, from Pan and Puls, performing a quasistatic study of hydride dissolution and measuring the

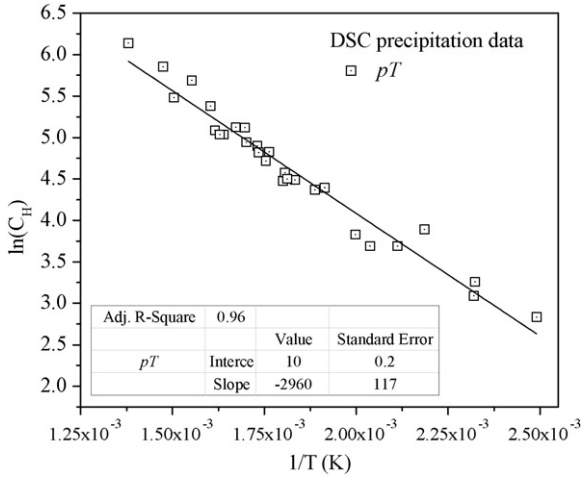

Fig. 8. vant Hoff plot made with the DSC precipitation data.

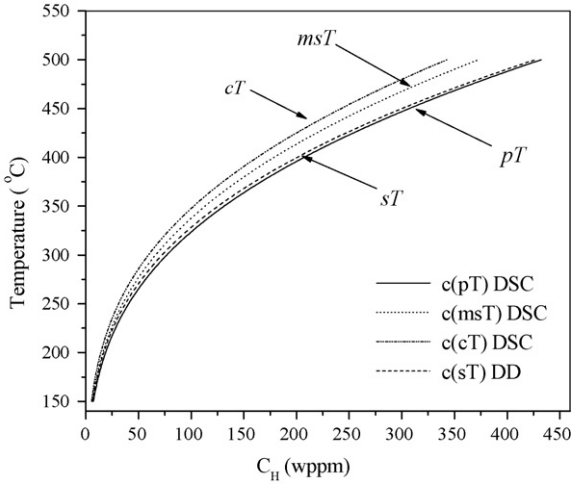

Fig. 9. Dissolution curves obtained by calorimetry and dilatometry.

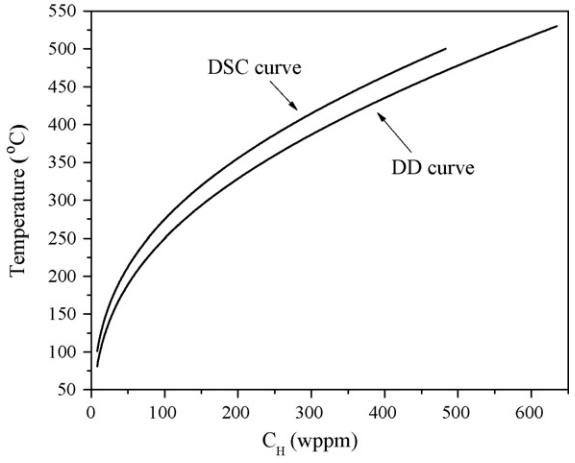

Fig. 10. Precipitation curves obtained by calorimetry and dilatometry.

Young modulus during heating runs concluded that the msT is the most reliable temperature from a practical point of view [4], since the remaining undissolved hydrides at this temperature are equivalent to the experimental error in the hydrogen concentration measurement (about 6 wppm). This implies that the TTSSd value will be the msT or a bit higher than it. On the other hand, Khatamian and Root, comparing DSC measurements with neutron diffraction results observing the disappearance of the (1 1 1) peak

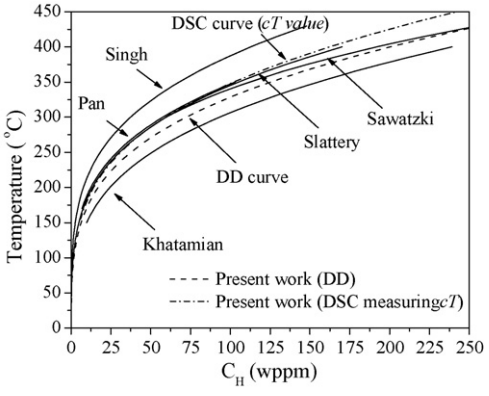

Fig. 11. Comparison of the dissolution curves obtained in the present work and some of the curves found in the literature.

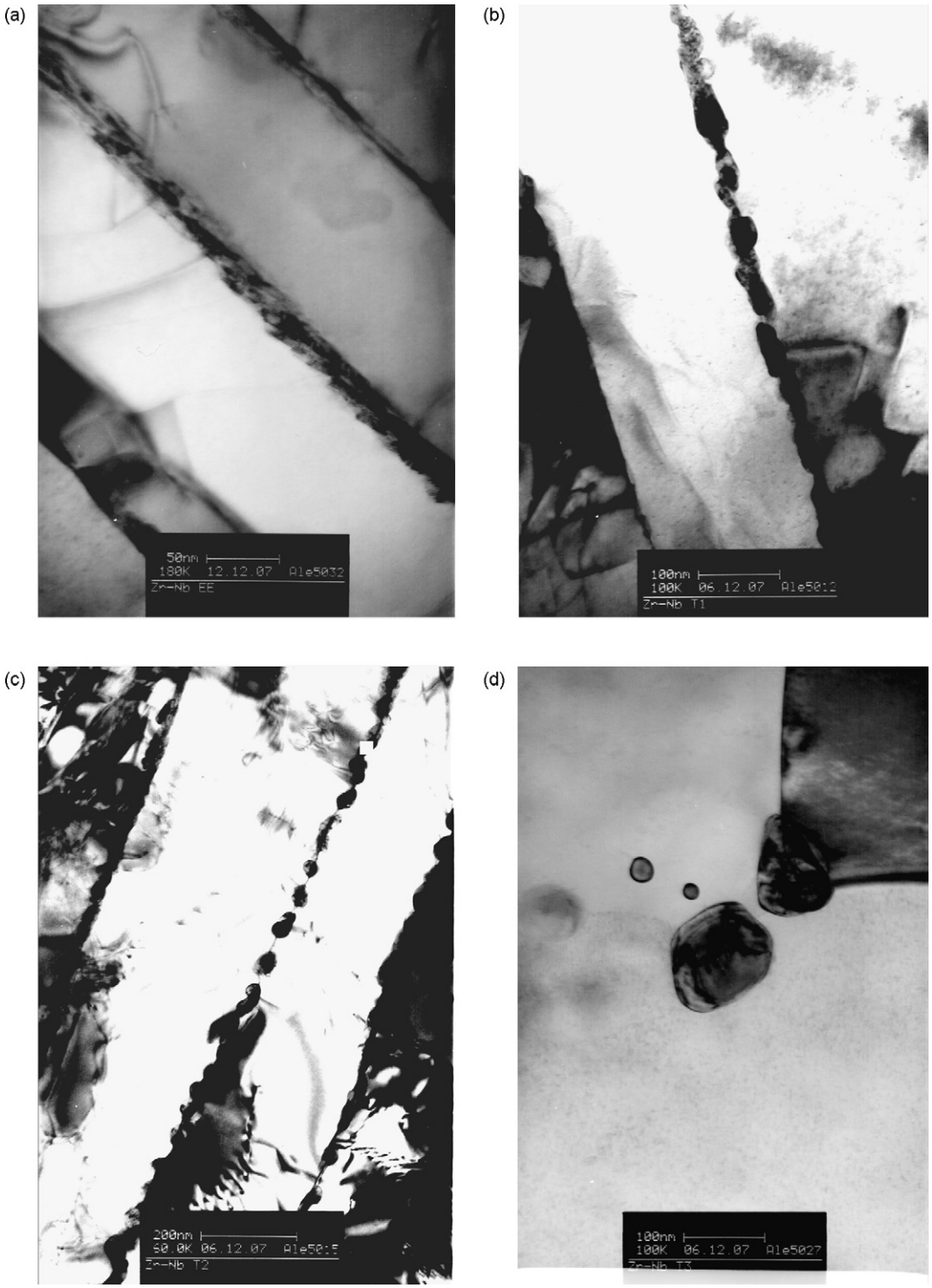

Fig. 12. (a) The original pressure tube microstructure, (b) after 30 min at 400 °C, no changes are observed, (c) after 1 h 30 min at 550 °C, β-Zr bands are discontinued and globular precipitates emerge, and (d) after 24 h at 550 °C, the globular β-Nb precipitates have the equilibrium composition 80%-Nb and 20%-Zr.

of the δ and γ-hydride during a heating run, concluded that the best one is the pT [3]. The ambiguity in relation to TTSS determinations still subsists.

The dissolution Eqs. (1–5) are drawn in Fig. 9.

5.2. Precipitation

We found that the dissolution–precipitation hysteresis varies between 30 and 50 °C. Fig. 10 shows the precipitation curves obtained from DD and DSC data and Fig. 11 show the dissolution curves obtained in the present work and some curves found in the literature.

The hydrogen concentration interval shown in Fig. 11 is similar to the one that cited authors considered in their works. The discrepancy between the DSC curve obtained measuring cT and the DD curve (virtually identical to the DSC one obtained measuring pT) is the highest of the four curves obtained in the present work. These curves were selected to show that in the gap between them

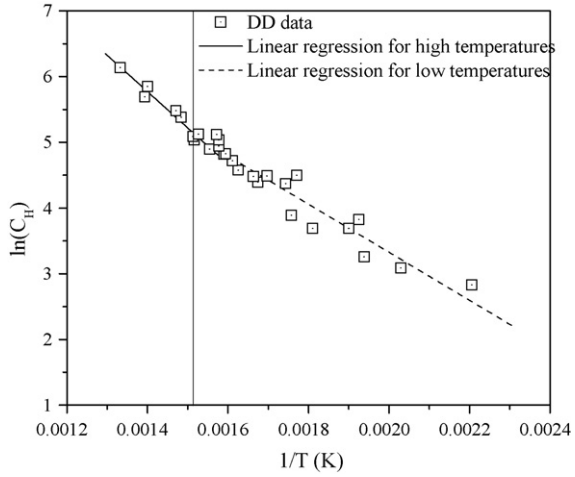

Fig. 13. vant Hoff plot for the dissolution data obtained by DD. The low and high concentration data were fitted separately.

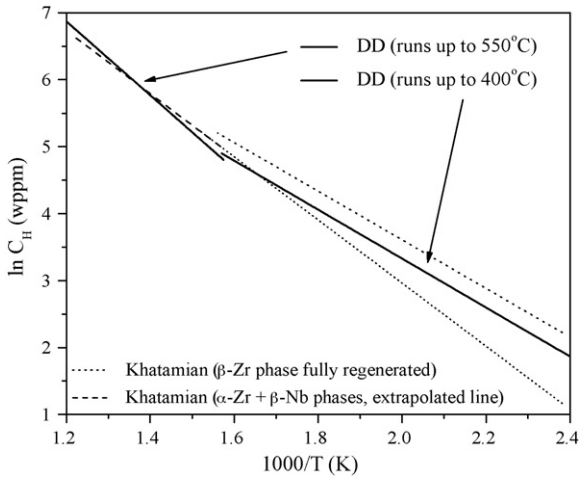

Fig. 14. Comparison with the Kathamian 1000 h aged material solvus line [6].

many of the most referenced curves are included. In addition, as can be seen in Fig. 11, the dispersion of the data of the present work is substantially smaller than the one observed in the literature.

The DSC curve obtained by measuring cT is close to the Pan, Sawatzki and Slattery curves up to 100 wppm, the typical range of interest for the pressure tube [7–9]. Surely, the internal friction data (IF) obtained by Pan are the most accurate ones. It has been said that Pan data come from the msT. As in the DSC case, this temperature is mathematically appropriate from an accuracy point of view, because the sharp peak of the derived curve reduces the experimental error. But examining the spread knee observed the E vs. temperature curve [4,7], things could change considerably if the measurement were made at pT. The reliability of the criterion selected for a TSS determination has turned decisive from an accurate determination of the solvus line, still using the more updated techniques.

Singh obtained the greatest TTSSd values. In his work he mentions this difference but he did not give any explanation [10] and Slattery performed thermal treatments to his samples at 500 °C during long periods (up to 70 h) which certainly decomposed the β-Zr phase. At temperatures above 400 °C the pressure tube microstructure begins to change. Since the β-Zr phase has a greater capacity to dissolve hydrogen than the α-Zr phase, the decomposition of the β-Zr phase has a non-negligible effect on the hydrogen solubility of the alloy, as it was showed by Khatamian [6,11]. In the TEM micrographs (Fig. 12a–d) the decomposition of the β-Zr bands is clearly shown: 1 h 30 min at 550 is enough to globulize the β-Zr (Fig. 12c). After 24 h at 550 the composition of the β-Zr phase is 20%-Zr and 80%-Nb, the expected for the phase β-Nb fully regenerated. This explains the change in the slope observed from 400 °C in the vant Hoff plots of Figs. 5–8.

In the plot of Fig. 13, the high concentration data were fitted separately by two regression lines: data from samples with hydrogen contents smaller than 180 wppm and higher than 180 wppm.

Further, with the aim of comparing the effect of the thermal treatments at 550 °C with the ones made by Khatamian in [6], the annealing cumulative parameter (CAP) was used [12,13].

$$\mathrm{CAP} = \sum_i t_i \exp\left(\frac{-Q}{RT_i}\right); \tag{7}$$

where t_i is the time at which the sample remained at the temperature T_i, and Q/R takes a value of 40,000 K for zirconium base alloys.

For the samples heated up to 550 °C (1 h, 30 min) the calculated value is 6.9×10^{-20}. This value is similar to an ageing made by Khatamian at 500 °C (773 K) during 1000 h (CAP = 3.4×10^{-20}) [6]. Actually, extrapolating Khatamian's line for this material to temperatures higher than 400 °C, the vant Hoff plot is similar to the one obtained in the present work, Fig. 14.

In the precipitation case, comparisons with other authors are rather difficult since TTSSp is very sensitive to the previous thermal history. Fig. 15 shows the precipitation curves obtained in the present work, which are compared with many curves found in literature. The comparison is made again for the low hydrogen region. A good example is the difference that can be observed in the curves obtained by Pan [7], cooling from different maximum temperatures ranges (from 220 to 370 °C in one case, and from 385 to 450 °C the other), Fig. 15.

The cooling rate is another factor, which affects the onset of the precipitation process. The supper-saturation needed to start precipitation is reduced, as the cooling rate is smaller. The differences between the dilatometric data obtained by Singh cooling at 2 °C/min and that of the present work cooling at 5 °C/min can explain in part the higher values obtained by Singh. The same can be said about Pan data, since he cooled down at 2 °C/min too. Another thing that should be considered in relation with Pan data is related to the point where TTSSp is measured. For the precipitation case,

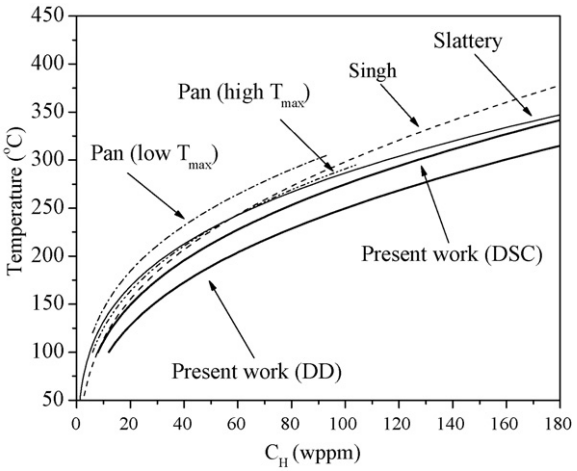

Fig. 15. Comparison between the precipitation curves of the present work and some that which can be found in the literature.

an increase of 5–10 °C in TTSSp values will arise if msT (Pan, IF) is measured instead of pT (present work, DSC). As expected, our cooling data of 400 °C are closer to the Pan high maximum temperature data.

Slattery's cooling data were obtained at a low cooling rate too (1.5 C°/min), but the different degree of decomposition of the β-Zr of his samples precludes the possibility of doing a deeper analysis.

Some words must be said in relation to the global difference found between DSC data and DD data in the present work. From a qualitative point of view (Figs. 1 and 2), the step in the DD differentiated curve is about 40 °C for the dissolution case, and 25 °C for the precipitation case. In the DSC curve (Figs. 3 and 4), the difference between pT and cT is about 25 °C for the dissolution case and 10 °C for the precipitation. It is clear that DSC is more accurate than DD for TSS determinations. Thus, the temperatures obtained by DD are highly dependant on the criterion selected to determine the solubility limits than the DSC ones. If for example, the left side of the step in the DD curve of Fig. 2 were chosen as the TTSSp point, the precipitation curve would be close to the DSC curve in Fig. 15. The selection of the sT temperature in the dilatometric case was strictly related with the experimental accuracy in the determination, which allowed to have the same dispersion that the DSC technique. Since the criterion depends on the sensitivity of the technique, this dilemma takes us to the problem of the physically meaningful criteria to measure the solubility limit. The disappearance of the neutron diffraction hydride peaks in [3] at pT implies that hydrides which are smaller than the detection limit of the technique will not be observed, that is to say, hydrides of about 50 nm or a bit larger (precipitates containing more than 100 atoms) will remain still undissolved at pT. On the other hand, internal friction is capable of detecting dimmers, that is, pairs of atoms, then, the shift of TSS to a high temperature, that is, msT *instead of* pT in [4] is not surprising, because IF is capable of detecting precipitate sizes that ND cannot resolve.

Perhaps, from a practical point of view, the criteria for TSS determinations should be associated to the hydride size that could be considered critical for DHC initiation. If hydrides of this critical size exist at the operating temperatures in the pressure tubes, it will be surely a big problem.

Another way apparently not followed yet is trying to modelize the TTSS phenomenon under a DSC or IF run condition, in order to see in which manner and for which factors (hydride size, sizes distribution, heating rates and so on) the recovery of the baseline acquires its shape. This type of information could give physical support to one of the criteria commonly followed for TSS determinations.

6. Conclusions

In the present work, the TTSS limits were measured by two techniques, DD and DSC. From a technological point of view, the hydrogen concentration interval of interest for pressure tubes is between a few wppm to about 100 wppm. In the present work, TSS measurements were extended up to 463 wppm. The solubility equations obtained from the dilatometric data are:

$$C_H(\text{ppm}) = 6.89 \times 10^4 \exp\left(\frac{-3930}{T(\text{K})}\right), \text{dissolution}$$

$$C_H(\text{ppm}) = 1.99 \times 10^4 \exp\left(\frac{-2768}{T(\text{K})}\right), \text{precipitation}$$

and the solubility equations obtained by DSC are:

$$C_H(\text{ppm}) = 6.11 \times 10^4 \exp\left(\frac{-3827}{T(\text{K})}\right), \text{dissolution}$$

$$C_H(\text{ppm}) = 2.22 \times 10^4 \exp\left(\frac{-2961}{T(\text{K})}\right), \text{precipitation}$$

Both equations were obtained from the TTSS values measured at pT.

The dissolution and precipitation enthalpies are 32.5 and 24 kJ/mol H, respectively (±1 kJ/mol H), in good agreement with the values found in the literature.

As was shown, for temperatures higher than 400 °C, which are required to dissolve hydrogen contents higher than 180–200 wppm, the gradual β-Zr decomposition cannot be ignored and the TSS determinations will be inevitably affected by this process, as was observed by DSC and DD data, supported by TEM studies.

The differences found between the curves obtained in the present work and the literature data must be attributed essentially to the different criteria selected for TSS determinations, at least for the most sensitive techniques like DSC or IF.

The recommendation of a unified criterion for TSS determinations supported by a practical consideration is made.

Acknowledgements

We are in debt with Drs. Hilda Lanza, Gabriela Leiva and Daniel Vega who facilitated the use of their DSC while ours was in maintenance. We are grateful to Dr. Yuh Fukai by his opinion and comments about the criteria used for TSS determinations. Finally we are thankful to Javier Palmerio and Ignacio Lopez Vergara for the hydrogen measurements and their support during the development of the work.

References

[1] A. Cheadle, S.A. Aldridge, Journal of Nuclear Materials 47 (1973) 255–258.
[2] M. Griffiths, J.E. Winegar, AECL-10835 COG-93-179 (1994).
[3] D. Khatamian, J.H. Root, Journal of Nuclear Materials 372 (1) (2008) 106–113.
[4] Z.L. Pan, M.P. Puls, Journal of Alloys and Compounds 310 (2000) 214–218.
[5] J.C. Ovejero, A.D. Banchik, P. Vizcaíno, Advances in Technology of Materials and Materials Processing Journal (ATM) 10 (2008) 1–8.
[6] D. Khatamian, Journal of Alloys and Compounds 293–295 (1999) 893–899.
[7] Z.L. Pan, I.G. Ritchie, M.P. Puls, Journal of Nuclear Materials 228 (1996) 226–237.
[8] A. Sawatzky, B.J.S. Wilkins, Journal of Nuclear Materials 22 (1967) 304–310.
[9] G.F. Slattery, Journal of the Institute of Metals 95 (1967) 43–47.
[10] R.N. Singh, S. Mukherjee, A. Gupta, S. Banerjee, Journal of Alloys and Compounds 389 (2005) 102–112.
[11] D. Khatamian, V.C. Ling, Journal of Alloys and Compounds 253–254 (1997) 162–166.
[12] J.H. Baek, Y.H. Jeong, I.S. Kim, Journal of Nuclear Materials 280 (2000) 235–245.
[13] K.T. Erwin, O. Delaire, A.T. Motta, Y.S. Chu, D.C. Mancini, R.C. Birtcher, Journal of Nuclear Materials 294 (2001) 299–304.